





Topological properties of interfacial hydrogen bond networks

Ruiyu Wang ^{1,2}, Mark DelloStritto ³, Michael L. Klein,^{1,2,3} Eric Borguet ^{1,2,*} and Vincenzo Carnevale ^{3,4,†}

¹*Department of Chemistry, Temple University, Philadelphia, Pennsylvania 19122, USA*

²*Center for Complex Materials from First Principles (CCM), Temple University,*

1925 North 12th Street, Philadelphia, Pennsylvania 19122, USA

³*Institute for Computational Molecular Science, Temple University, Philadelphia, Pennsylvania 19122, USA*

⁴*Department of Biology, Temple University, Philadelphia, Pennsylvania 19122, USA*



(Received 23 September 2023; revised 8 June 2024; accepted 11 June 2024; published 15 July 2024)

Hydrogen bonds play a crucial role in the anomalous behavior of water. While the properties of individual hydrogen bonds have been extensively studied, the topological characteristics of the resulting hydrogen bond network remain less explored. In this study, we employ molecular dynamics simulations to examine various aqueous interfaces, uncovering an increased number of hydrogen bonds parallel to surfaces compared to bulk water. To quantify the topology of these networks, we introduce estimators for network percolation and dimensionality. Our findings reveal that the elevated proportion of hydrogen bonds parallel to the interface significantly influences network connectivity, reducing both the number of water layers and the distance from the surface at which the network achieves full connectivity. Consequently, hydrogen bond networks at interfaces exhibit more “two-dimensional” characteristics than those in bulk water due to high local water density and the competition between water-water hydrogen bonds and water-surface interactions.

DOI: [10.1103/PhysRevB.110.014105](https://doi.org/10.1103/PhysRevB.110.014105)

I. INTRODUCTION

Understanding and controlling interfacial phenomena is essential for a wide range of applications, including catalysis, electrochemistry, dissolution, corrosion, and electrochemical energy storage [1–9]. A fundamental question about interfacial phenomena concerns the origin of their distinct properties: how do these properties depend on the structure of the solid and liquid components? The question is especially pertinent for aqueous interfaces, as strong hydrogen bonds (hydrogen bonds) of water result in a structured liquid with anomalous behaviors, such as a high boiling point and surface tension [10,11]. The fluctuation of hydrogen bonds also play a critical role in driving proton transfer in water [12–18].

In bulk water, each water molecule forms an average of 3.5 hydrogen bonds [19], much higher than the percolation threshold of a 3D network [20]. This suggests the presence of an isotropic and homogeneous hydrogen bond network connecting all waters without a preferred orientation [21–23]. However, hydrogen bond networks at interfaces often differ substantially from those in bulk water [1]. For instance, at the water/air interface, the vacuum allows free unbonded OH groups to be perpendicular to the surface and point toward the air [24–26]. Hydrogen bonds between interfacial waters tend to be parallel to the surface, resulting in a connected hydrogen bond network at the topmost layer of the interface [27–29]. Besides planar surfaces, water/protein interfaces exhibit a monolayer of protein hydration that displays “quasi-2D percolation,” a phenomenon believed to be related to proteins’ biofunctions [30–32].

Previous research has focused on individual hydrogen bonds [33] and their perturbation by solute molecules [24]. However, quantitative descriptions for the entire hydrogen bond network at interfaces are missing. To compare the entire network at different interfaces and differentiate it from bulk water, we propose universal network descriptors using graph based approaches to characterize the 2D density-dependent connectivity of water at water/air, α -alumina(0001), modified graphene, Pt(111) surfaces, and the cut-bulk surface [34–39]. Additional details to model the surfaces are discussed in the Supplemental Material [40] (SM, see also Refs. [4,10,30,41–61] therein). These surfaces are charge neutral, possessing both hydrophilic and hydrophobic character. Interfacial waters interact strongly with the alumina surface but weakly with all other surfaces [62–64]. The modified graphene surface contains alternative positive and negative charges on the carbon atoms, showing both hydrophilic and hydrophobic behaviors [43]. Simulation results demonstrate that interfacial water hydrogen bond networks are more densely connected than those in bulk water. Although this property holds true for all surfaces, we observe quantitative variations stemming from the hydrophilicity of surfaces and the local water density.

To comprehensively investigate the nature of an interface, it is imperative to accurately define its dimension. This task is challenging especially for liquid-liquid interfaces and liquid-vapor interfaces that often exhibit intricate shapes with ambiguously delineated boundaries. To estimate the dimensionality of the interface it is necessary to develop a method to estimate the dimensionality of an arbitrary arrangement of molecules. One effective strategy is to take advantage of the scaling laws, where the intrinsic dimension of the space is deduced from the limit of the cumulative distribution of pair distances as the distance approaches zero [65]. Unfortunately,

*Contact author: eborguet@temple.edu

†Contact author: vincenzo.carnevale@temple.edu

complex manifolds of points and noise can cause problems with the estimation of the dimension [61]. An alternative approach is to compute the intrinsic dimension of a set of points by using the geodesic distances, which measures the length of the pathways between points using only nearest-neighbor graph distances. This method yields accurate intrinsic dimensions regardless of the shape of the manifold of points [61]. Consequently, the approach can be employed to assess the intrinsic dimension of a molecule set situated at an interface.

While measuring the intrinsic dimension of a molecular system is an excellent technique to determine its overall shape, the structure of the hydrogen bond network is ignored. Methods to measure the intrinsic dimension work on a series of points in N dimensions. In the context of water, these points correspond to the positions of the water molecules, defined by the positions of the oxygen (O) atoms. As each water molecule frequently both accepts and donates hydrogen bonds to its neighbors, water can be treated as a dynamic percolation network. An alternative strategy to assess the structure of an aqueous interface involves investigating the connectivity of interfacial water and the path of their hydrogen bond network.

Anticipating our results, we find that we can accurately measure the change of dimension of interfacial water using the intrinsic dimension, defined as the dimension of a minimal representation of a molecular structure. While there are small deviations in the intrinsic dimension between interfaces, the dimension shows similar behavior for all interfaces, and can take several nanometers to converge to bulk values.

The connectivity of an hydrogen bond network at interfaces generally yields more information than the dimensionality. While 2D densities are the same at the surfaces investigated in this work, the interfacial hydrogen bond network has higher connectivity than that of bulk water. The size of connected components formed by the hydrogen bond networks are very different for different interfaces, illustrating the importance of the competition between interactions, which defines interfacial behaviors.

II. RESULTS AND DISCUSSIONS

A. Intrinsic dimensions of interfacial water

It is important to determine whether the width of the interfacial region differs between various interfaces with different materials. We identify the location and thickness of the interfaces using the dimensionality, that is, where the bulk liquid ends, and the interfacial region begins. We measure the size of the interface by computing the intrinsic dimension of the interface as a function of depth from the point at which the density drops below 10^{-6} nm^{-3} . The intrinsic dimension can be thought of as the dimension of a minimal description for a set of data. To make this idea more concrete, when applied to structures, the intrinsic dimension can be thought of as the fewest number of dimensions required to specify all points of the structure. For example, consider a sheet of graphene and a carbon nanotube, where it might at first appear that the two structures have different dimensions. The graphene sheet is flat and fits in a 2D plane and thus has a dimension of 2, while on the other hand the carbon nanotube has a width, height, and length and thus would appear to have a dimension of 3. However, note that both structures can be fully described using only 2 variables: the graphene sheet by the x-y displace-

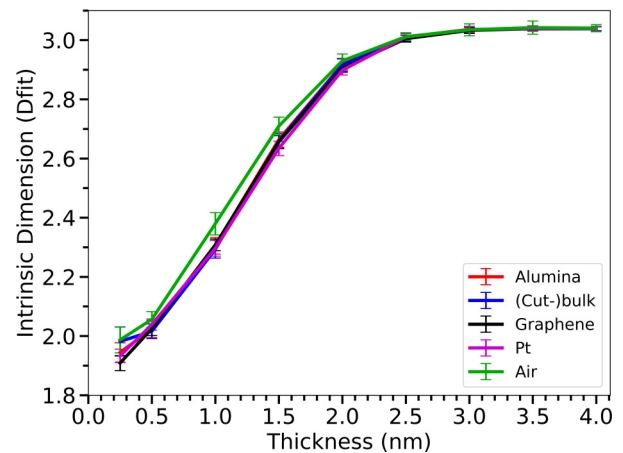


FIG. 1. Plot of the intrinsic dimension of different water interfaces as a function of the depth of the interface from the point of zero density.

ment, and the carbon nanotube by the angular and longitudinal displacement. Thus, while the sheet and the tube require a different number of Cartesian dimensions, their intrinsic dimension is the same. One can define the intrinsic dimension for any set of points using a graph distance approach [61]. We use this method to obtain the intrinsic dimension of a group of water molecules by using the Oxygen positions as the inputs for the intrinsic dimension estimator.

As expected, the intrinsic dimension as a function of depth (Fig. 1) for interfaces between water and a range of different materials rises from an initial value of approximately two to an asymptotic value of approximately three over a distance of about 3 nm, which matches the thickness of interfaces inferred from density fluctuations [59]. While there are some slight differences between the profiles of different interfaces, they overall exhibit a remarkable similarity. This is particularly surprising for the more flexible air/water interface, which has some fluctuations out of the plane of the interface, in contrast to interfaces with rigid bulk materials like alumina and platinum. Thus, while the dimensionality of the interface is well defined and reproduces results from other measures of the interface, it does not yield any insight into the nature of the hydrogen bond network at various interfaces. This is most likely because the intrinsic dimension of a set of points is defined by graph distances without any directionality, and this ignores the directional nature of the hydrogen bonds between water molecules.

B. Density and orientation of hydrogen bonds between interfacial waters

A perfect, isolated 2D hydrogen bond network requires that all water molecules reside within the same plane, akin to the structure of 2D ice [66–68]. The configuration gives rise to a δ -like function representing the local density of water oxygen atoms. However, in this work, such an ideal, well-structured arrangement has not been observed. Only at the Pt surface is the water density between the first two peaks close to zero. The density of this region at the graphene and alumina surfaces is reduced but still higher than zero (Fig. 2). The first peak of the local water density is significantly higher than

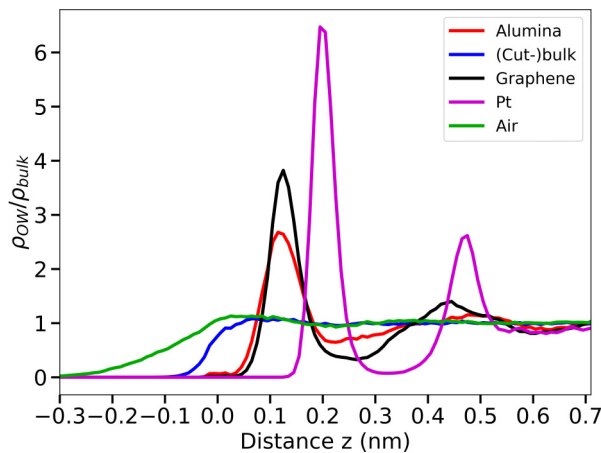


FIG. 2. Density profile (normalized to bulk water) of interfacial water molecules at the five surfaces studied in this work. “Distance z ” represents the distance between water and the instantaneous surfaces. The left and right sides represent surface and bulk directions, respectively.

the bulk liquid at alumina, Pt(111), and graphene surfaces, suggesting a possible competition between hydrogen bonds parallel and perpendicular to the surface. As for the cut-bulk surface, the reference system with 3D behavior, the density profile shows no pronounced peaks. Since the distance between two peaks of water local density at Pt surface is less than 0.3 nm and hydrogen bonds between the two layers still persist, the interfacial hydrogen bond network is not isolated from bulk waters. Nevertheless, it is inadequate to conclude that the water hydrogen bond network at Pt surfaces shows 2D behavior based on water density profile only.

Another characteristic of a perfect 2D hydrogen bond network is that all hydrogen bonds are flat and parallel to the surface, which can be assessed using the probability distribution of hydrogen bond orientations. In bulk water, hydrogen bonds exhibit no preferred orientation, allowing their network to expand into all three dimensions. Conversely, hydrogen bond networks tend to expand parallel rather than perpendicular to the surfaces. The distribution of hydrogen bond orientation [Figs. 3(a) and 3(b)], $P(\cos\phi, z)$, of interfacial water shows that near the cut-bulk surface [Fig. 3(d)], the count of hydrogen bonds perpendicular to the surface diminishes. This decline can be attributed to the removal of water beyond the surface, along with the associated cross-surface hydrogen bonds, which are likely oriented perpendicular to the surface. The hydrogen bond network is considered to have reduced dimensionality if it has more parallel hydrogen bonds than the reference cut-bulk surface.

The hydrogen bond network at the water/air interface is not isolated, as indicated by a distinct area within $|\cos\phi| < 0.5$ and a thickness less than 0.2 nm [Fig. 3(f)]. The observation suggests that interfacial waters remain connected with bulk water, even though a higher number of hydrogen bonds exist within the first layer at $0.2 < z < 0.3$ nm compared to bulk water. At the alumina, graphene, and Pt(111) surfaces that are characterized by higher local density, a significant number of hydrogen bonds parallel to the surfaces are observed, making the $P(\cos\phi, z)$ show a “K” pattern (Fig. 3).

These interfacial hydrogen bonds are flatter ($|\cos\phi| < 0.4$) than those at the water/air interface and the thickness of the hydrogen bond network is only about 0.1 nm as a result of high water local density that forces waters to form flat hydrogen bonds. Similar behaviors have been observed for ions under 2D confinement, which tend to be paired, forming a crystal rather than a solution [69]. The hydrogen bond density in the region $0.2 < z < 0.4$ nm for both $P(\cos\phi, z)$ and $P(\cos\phi|z)$ show the trend Pt > graphene > alumina (Figs. 3 and S2), indicating pronounced hydrogen bond network isolation. That is, waters in this layer prefer hydrogen bonds within the layer rather than other layers. This phenomenon occurs at the Pt surface and is the weakest at the alumina surface, consistent with their local water density. At all surfaces in this work, hydrogen bond networks of interfacial waters that display behaviors of reduced dimensionality, such as parallel orientational and low density of interlayer hydrogen bonds, are observed with an increased water local density.

C. Topology of interfacial hydrogen bond networks

1. Universal enhanced connectivity and reduced dimensionality

The whole hydrogen bond network also shows characteristics of reduced dimensionality. To assess the network connectivity quantitatively, the “maximum connected ratio” (MCR) is introduced as the ratio between the size of the maximum connected component (N_{MCC}) and the number of interfacial waters (N):

$$\text{MCR} = \frac{N_{MCC}}{N}. \quad (1)$$

The highest possible value of MCR is 1, when all interfacial waters are completely connected. The water 2D density (number of water per nm^2) is chosen as the independent variable and it is correlated with the thickness of the water slab (Fig. S3). Even in bulk water, increasing the thickness of water slab or the water number 2D density results in a higher MCR value, consistent with the fact that in bulk water nearly all waters are connected via hydrogen bonds. To eliminate the influence of small, isolated clusters, we adopt $\text{MCR} = 0.95$, i.e., when 95% of waters are connected in the hydrogen bond network, as the threshold for connected. Comparing to the cut-bulk surface, fewer waters per unit area are required to reach the threshold of the connected state at all other surfaces (Fig. 4), in other words, each water occupies the larger space in the 2D plane.

The graphene and Pt(111) surfaces, characterized by high local water density, require the fewest waters to be connected, displaying the most pronounced 2D characteristics. The 2D behavior near the alumina surface appears considerably weaker. In contrast to other surfaces that lack surface-water hydrogen bonds, waters donate strong hydrogen bonds to aluminol groups, which compete with water-water hydrogen bonds, making water orientation perpendicular to the surface and disrupting the 2D behavior of interfacial hydrogen bond network (Fig. 4) [63].

Based on these observations, 2D behaviors of hydrogen bond networks are determined by two key factors. First, weak interactions between interfacial water and a surface promote 2D behaviors of the hydrogen bond network, due to the challenge of maintaining a 3D hydrogen bond network with-

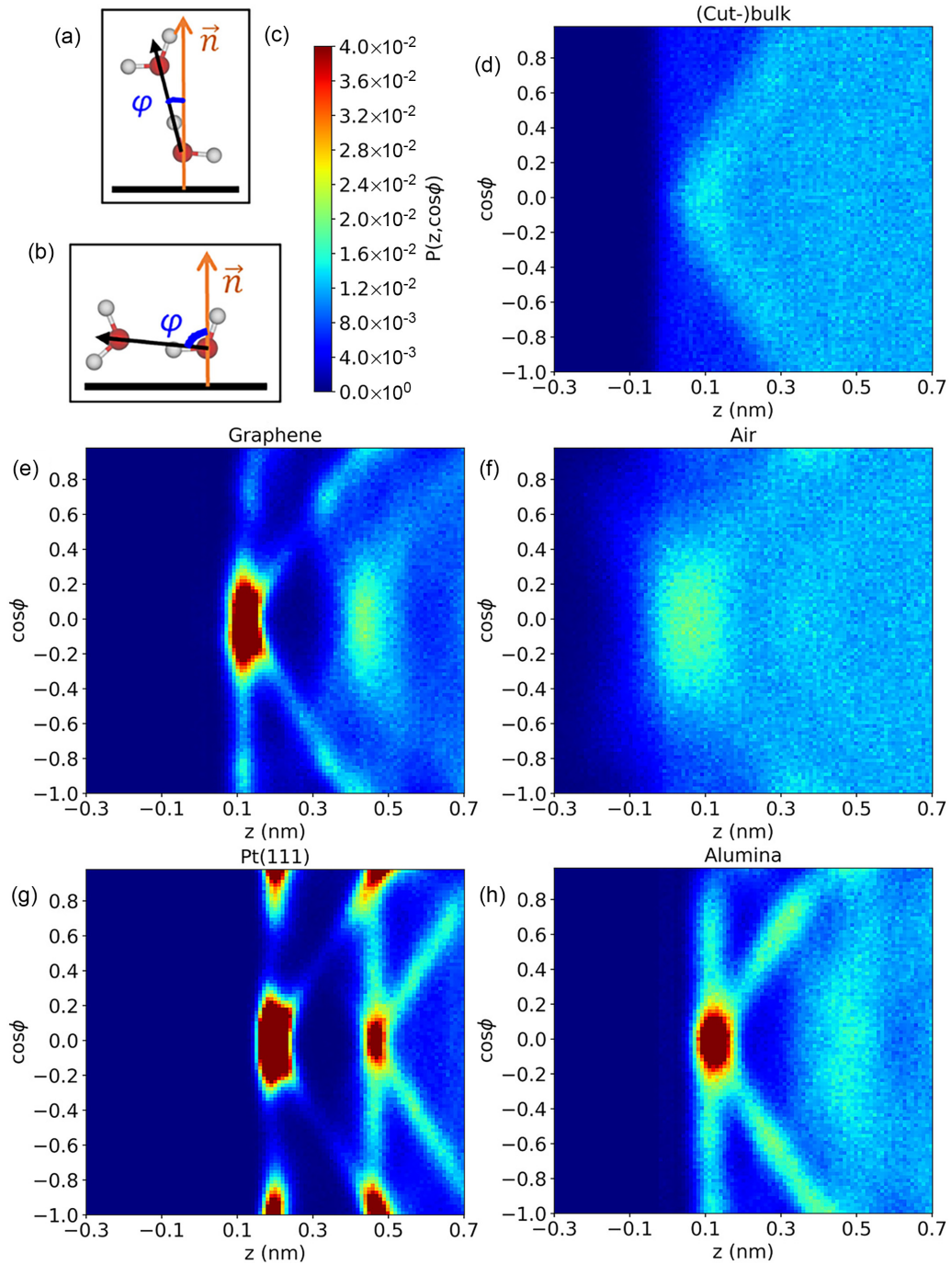


FIG. 3. Distribution of hydrogen bond orientations of interfacial waters. (a), (b) Definition of the hydrogen bond orientation angle; more details are discussed in the SM. (c) Color code used for heatmaps. (d)-(h) Joint probability $P(\cos\phi, z)$ for the five surfaces. The label z of x axes represents the distance between a water molecule and the instantaneous surface.

out water-surface hydrogen bonds, as waters do not prefer free OH groups [70]. Second, water adsorption at surfaces increases the local density, forcing waters to be connected via in-plane hydrogen bonds.

The dimensionality can be effectively characterized using a metric that captures the rate at which hydrogen bond networks expand in the third dimension. The speed of MCR growth is fit using

$$y = a * \tanh(b * x + c) + 1 - a, \quad (2)$$

where the coefficient b describes the growth rate of MCR. Among all surfaces, the b value of cut bulk is the smallest, consistent with the 3D behavior of bulk water. The MCR at other surfaces grows significantly faster than bulk water except for the Pt(111) surface whose low growth is attributed to the high local water density. When fitting the MCR to the thickness of hydrogen bond networks, growth at the Pt(111) surface is the fastest among all surfaces and that of bulk water is still the lowest (Fig. S3). Although the b value alone is not a perfect indicator of the 2D behavior of networks, it

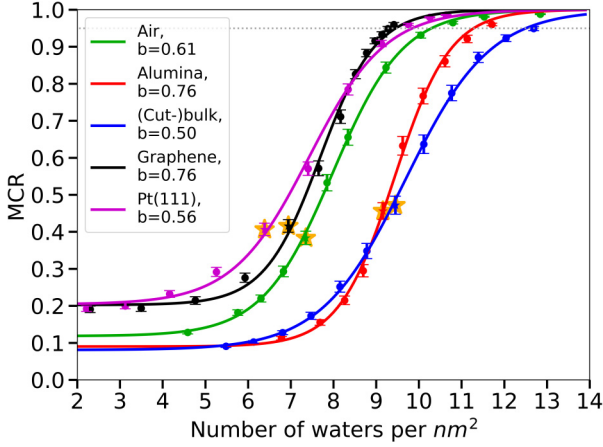


FIG. 4. The maximum connected component (MCR) value versus number of waters per nm^2 for all surfaces investigated. The gray dotted line at the top is $\text{MCR} = 0.95$, the threshold of a fully connected water slab. All other colored markers are directly calculated from simulation trajectories and all curves are fit using Eq. (2). Yellow star markers represent the critical percolation points.

offers indirect evidence for enhanced 2D behaviors for these surfaces.

2. Universal critical points of connectivity percolation transition

We also observed 2D percolation behaviors at all interfaces and a uniform percolation critical point in Fig. 4. At the critical point, we expected the power law of the probability distribution [$P(n)$] of the sizes of water clusters (n) to follow

$$P(n) \sim n^{-\tau}, \quad (3)$$

where $\tau = 187/91 \approx 2.055$ is the two dimension critical Fisher exponent [71,72]. For each thickness at each surface, we compute $P(n)$ and perform linear regression between $\log P(n)$ and $\log n$. The Pearson correlation coefficients (R^2) for all surfaces (Fig. S5) show that at very low thickness, a high R^2 is observed because there are not many water molecules. The exponential cut-off correction is expected to be significant only when n is high. The largest cluster sizes at these thickness are on the order of a dozen and are less by an order of magnitude compared to those at the critical percolation points, as shown in plots $P(n)$ with n for each thickness (Figs. S10–S14). As a result, instead of selecting the maximum R^2 , in this work, the thinnest water slab with $R^2 < 0.95$ is chosen as the critical point for each surface. Further increasing the thickness of water slabs leads to a rapid decrease in R^2 . This sharp change in the behavior of R^2 is another piece of evidence that the percolation phase transition occurs at these points. R^2 continues to decrease with increased thickness because, above the percolation threshold, large clus-

ters containing most water molecules are observed, resulting in a bimodal distribution of $P(n)$. At these critical points, all τ values obtained from Eq. (3) are around 2 (Table I), consistent with the two dimensional critical Fisher exponent [72]. Last, the percolation critical points occur at about $\text{MCR}=0.4$ (Fig. 4) for all interfaces and we believe that it is a universal behavior of 2D hydrogen bond networks of interfacial water.

3. Enhanced connectivity slows down dynamics of interfacial water

The dynamics of interfacial water is also compared (Fig. S8). The interfacial region is divided into four layers by the distance to surfaces (defined in Table S3). In this work, the mean square displacement (MSD) on x and y directions is applied to describe water dynamics parallel to surfaces [Eq. (4)]

$$\text{MSD}_{2d}(t) = \langle |x(t) - x(0)|^2 + |y(t) - y(0)|^2 \rangle. \quad (4)$$

In these calculations, the layers of water molecules are determined by their initial positions. The MSD data reveals that at Layer 0 and Layer 1, water dynamics are faster at water/air interfaces but slower at other solid surfaces, because surface-water interactions restrict the movement of water molecules, whereas there is no such interaction between water and vacuum. The water dynamics at cut-bulk surfaces are the same at all layers because removing waters on one side after simulations for analysis does not affect the movement of individual water molecules. At solid interfaces, Layer 2 and Layer 3 are less affected by solid surfaces. Diffusion in the two layers are similar and comparable with the bulk. The continuous water residence autocorrelation function describes the movement of water perpendicular to surfaces [63], and is defined by

$$R(t) = \frac{\langle r(0)r(t)s_r(t) \rangle}{\langle r(0)r(0) \rangle}, \quad (5)$$

$$s_r(t) = \prod_{i=0}^t r(i), \quad (6)$$

where $r(t)$ could be 1 or 0, representing whether a water molecule is in or out of a specific layer, respectively. $R(t)$ exhibits a similar trend as the 2D MSD: water molecules that move faster parallel to surfaces also do so perpendicularly. The only exception is Layer 2 at the water/Pt interface, where $R(t)$ decays slower and close to Layer 1 instead of Layer 3 at other solid interfaces. Also, only Layer 0 at the water/air interface contains enough number of water molecules. At the solid surface, the layer is thin and cannot hold water. There is no water observed at Layer 0 for the Pt surface.

TABLE I. τ values and thicknesses (nm) at each surface at the critical point.

Surface	Air	Alumina	(Cut)bulk	Graphene	Pt(111)
Thickness	0.12	0.24	0.26	0.15	0.205
τ	1.894	1.575	1.638	1.733	1.811

III. CONCLUSION

In summary, we explored the topology of hydrogen bond networks at the air, α -alumina(0001), modified graphene, and Pt(111) surfaces and compared them with the cut-bulk surface as a model of a 3D hydrogen bond network. All surfaces show similar dimensionality, though it can take several nanometers for the intrinsic dimension to converge to the bulk value. In addition, at all surfaces compared to the cut-bulk one, interfacial waters exhibit more hydrogen bonds parallel to the surfaces. Using MCR and MCR growth as the metrics of connectivity, we find that hydrogen bond networks at all other surfaces need fewer waters to reach a connected graph, showing increased connectivity and reduced dimensionality at interfaces. Surfaces with higher local water density and lower hydrophilicity show a more substantial reduction of dimensionality. Notably, the methodology we developed is not limited to planar surfaces and can be applied to water/protein and other soft surfaces. This adaptability allows for the exploration of interfacial hydrogen bond networks and how the networks affect the chemistry and physics at the surfaces. In addition, developing advanced graph based models to describe

interfacial water is also necessary to understand the structure and dynamics of phase transition of liquid water [39,73].

ACKNOWLEDGMENTS

This work was supported as part of the Center for Complex Materials from First Principles (CCM), an Energy Frontier Research Center funded by the U.S. Department of Energy, Office of Science, Basic Energy Sciences under Award No. DE-SC0012575. This research includes calculations carried out on HPC resources supported in part by the National Science Foundation through major research instrumentation Grant No. 1625061 and by the U.S. Army Research Laboratory under Contract No. W911NF-16-2-0189. E.B. acknowledges the support of the National Science Foundation under Grant No. CHE 2102557. V.C. acknowledges the support of National Institute of General Medical Science through Grant No. 5R01GM093290. M.D. Acknowledges support from the Computational Chemical Sciences Center: Chemistry in Solution and at Interfaces (CSI), which is funded under DOE Award No. DE-SC0019394.

-
- [1] O. Björneholm, M. H. Hansen, A. Hodgson, L.-M. Liu, D. T. Limmer, A. Michaelides, P. Pedevilla, J. Rossmeisl, H. Shen, G. Tocci, E. Tyrode, M.-M. Walz, J. Werner, and H. Bluhm, Water at interfaces, *Chem. Rev.* **116**, 7698 (2016).
- [2] J. Xu, M. Chen, C. Zhang, and X. Wu, First-principles study of the infrared spectrum in liquid water from a systematically improved description of H-bond network, *Phys. Rev. B* **99**, 205123 (2019).
- [3] R. Mu, Z.-j. Zhao, Z. Dohnálek, and J. Gong, Structural motifs of water on metal oxide surfaces, *Chem. Soc. Rev.* **46**, 1785 (2017).
- [4] R. Wang, M. L. Klein, V. Carnevale, and E. Borguet, Investigations of water/oxide interfaces by molecular dynamics simulations, *WIREs Computational Molecular Science* **11**, e1537 (2021).
- [5] J. L. Bañuelos, E. Borguet, J. Brown, G. E. Brown, Jr., R. T. Cygan, J. J. DeYoreo, P. M. Dove, M.-P. Gaigeot, F. M. Geiger, J. M. Gibbs, V. H. Grassian, A. G. Ilgen, Y.-S. Jun, N. Kabengi, L. Katz, J. D. Kubicki, J. Lützenkirchen, C. V. Putnis, R. C. Remsing, K. M. Rosso *et al.*, Oxide- and silicate-water interfaces and their roles in technology and the environment, *Chem. Rev.* **123**, 6413 (2023).
- [6] S. M. Piontek and E. Borguet, Vibrational spectroscopy of geochemical interfaces, *Surf. Sci. Rep.* **78**, 100606 (2023).
- [7] P. Xu, R. Wang, H. Zhang, V. Carnevale, E. Borguet, and J. Suntivich, Cation modifies interfacial water structures on platinum during alkaline hydrogen electrocatalysis, *J. Am. Chem. Soc.* **146**, 2426 (2024).
- [8] C. Penschke, J. Thomas, C. Bertram, A. Michaelides, K. Morgenstern, P. Saalfrank, and U. Bovensiepen, Hydration at highly crowded interfaces, *Phys. Rev. Lett.* **130**, 106202 (2023).
- [9] N. Di Pasquale, A. R. Finney, J. D. Elliott, P. Carbone, and M. Salvalaglio, Constant chemical potential–quantum mechanical–molecular dynamics simulations of the graphene–electrolyte double layer, *J. Chem. Phys.* **158**, 134714 (2023).
- [10] A. Luzar and D. Chandler, Hydrogen-bond kinetics in liquid water, *Nature (London)* **379**, 55 (1996).
- [11] Z. A. Piskulich, D. Laage, and W. H. Thompson, On the role of hydrogen-bond exchanges in the spectral diffusion of water, *J. Chem. Phys.* **154**, 064501 (2021).
- [12] R. Wang, V. Carnevale, M. L. Klein, and E. Borguet, First-principles calculation of water pK_a using the newly developed SCAN functional, *J. Phys. Chem. Lett.* **11**, 54 (2020).
- [13] P. L. Geissler, C. Dellago, D. Chandler, J. Hutter, and M. Parrinello, Autoionization in liquid water, *Science* **291**, 2121 (2001).
- [14] A. Hassanali, F. Giberti, J. Cuny, T. D. Kuhne, and M. Parrinello, Proton transfer through the water gossamer, *Proc. Natl. Acad. Sci. USA* **110**, 13723 (2013).
- [15] V. Quaranta, M. Hellström, and J. Behler, Proton-transfer mechanisms at the water-ZnO interface: The role of presolvation, *J. Phys. Chem. Lett.* **8**, 1476 (2017).
- [16] S. Di Pino, Y. Perez Sirkin, U. N. Morzan, V. M. Sánchez, A. Hassanali, and D. A. Scherlis, Water self-dissociation is insensitive to nanoscale environments, *Angew. Chem. Int. Ed.* **62**, e202306526 (2023).
- [17] D. Muñoz-Santiburcio and D. Marx, Nanoconfinement in slit pores enhances water self-dissociation, *Phys. Rev. Lett.* **119**, 056002 (2017).
- [18] M. Calegari Andrade, R. Car, and A. Selloni, Probing the self-ionization of liquid water with *ab initio* deep potential molecular dynamics, *Proc. Natl. Acad. Sci. USA* **120**, e2302468120 (2023).
- [19] R. Kumar, J. R. Schmidt, and J. L. Skinner, Hydrogen bonding definitions and dynamics in liquid water, *J. Chem. Phys.* **126**, 204107 (2007).

- [20] M. K. Horton and M. A. Moram, Alloy composition fluctuations and percolation in semiconductor alloy quantum wells, *Appl. Phys. Lett.* **110**, 162103 (2017).
- [21] A. Geiger, F. H. Stillinger, and A. Rahman, Aspects of the percolation process for hydrogen-bond networks in water, *J. Chem. Phys.* **70**, 4185 (1979).
- [22] S. Naserifar and W. A. Goddard III, Liquid water is a dynamic polydisperse branched polymer, *Proc. Natl. Acad. Sci. USA* **116**, 1998 (2019).
- [23] R. L. Blumberg, H. E. Stanley, A. Geiger, and P. Mausbach, Connectivity of hydrogen bonds in liquid water, *J. Chem. Phys.* **80**, 5230 (1984).
- [24] F. Tang, T. Ohto, S. Sun, J. R. Rouxel, S. Imoto, E. H. G. Backus, S. Mukamel, M. Bonn, and Y. Nagata, Molecular structure and modeling of water-air and ice-air interfaces monitored by sum-frequency generation, *Chem. Rev.* **120**, 3633 (2020).
- [25] M. Bonn, Y. Nagata, and E. H. G. Backus, Molecular structure and dynamics of water at the water-air interface studied with surface-specific vibrational spectroscopy, *Angew. Chem. Int. Ed.* **54**, 5560 (2015).
- [26] T. Ohto, M. Dodia, J. Xu, S. Imoto, F. Tang, F. Zysk, T. D. Kuhne, Y. Shigeta, M. Bonn, X. Wu, and Y. Nagata, Accessing the accuracy of density functional theory through structure and dynamics of the water-air interface, *J. Phys. Chem. Lett.* **10**, 4914 (2019).
- [27] A. Serva, S. Pezzotti, S. Bougueroua, D. R. Galimberti, and M.-P. Gaigeot, Combining ab-initio and classical molecular dynamics simulations to unravel the structure of the 2D-HB-network at the air-water interface, *J. Mol. Struct.* **1165**, 71 (2018).
- [28] S. Pezzotti, A. Serva, F. Sebastiani, F. S. Brigiano, D. R. Galimberti, L. Potier, S. Alfarano, G. Schwaab, M. Havenith, and M.-P. Gaigeot, Molecular fingerprints of hydrophobicity at aqueous interfaces from theory and vibrational spectroscopies, *J. Phys. Chem. Lett.* **12**, 3827 (2021).
- [29] A. Tuladhar, S. Dewan, S. Pezzotti, F. S. Brigiano, F. Creazzo, M.-P. Gaigeot, and E. Borguet, Ions tune interfacial water structure and modulate hydrophobic interactions at silica surfaces, *J. Am. Chem. Soc.* **142**, 6991 (2020).
- [30] A. Oleinikova, I. Brovchenko, N. Smolin, A. Krukau, A. Geiger, and R. Winter, Percolation transition of hydration water: From planar hydrophilic surfaces to proteins, *Phys. Rev. Lett.* **95**, 247802 (2005).
- [31] M.-C. Bellissent-Funel, A. Hassanali, M. Havenith, R. Henchman, P. Pohl, F. Sterpone, D. van der Spoel, Y. Xu, and A. E. Garcia, Water determines the structure and dynamics of proteins, *Chem. Rev.* **116**, 7673 (2016).
- [32] A. Arsiccio, J. McCarty, R. Pisano, and J.-E. Shea, Heightened cold-denaturation of proteins at the ice-water interface, *J. Am. Chem. Soc.* **142**, 5722 (2020).
- [33] S. Pezzotti, D. R. Galimberti, and M.-P. Gaigeot, 2D H-bond network as the topmost skin to the air-water interface, *J. Phys. Chem. Lett.* **8**, 3133 (2017).
- [34] J.-H. Choi, H. Lee, H. R. Choi, and M. Cho, Graph theory and ion and molecular aggregation in aqueous solutions, *Annu. Rev. Phys. Chem.* **69**, 125 (2018).
- [35] B. L. Mooney, L. R. Corrales, and A. E. Clark, Molecular networks: An integrated graph theoretic and data mining tool to explore solvent organization in molecular simulation, *J. Comput. Chem.* **33**, 853 (2012).
- [36] J.-H. Choi and M. Cho, Ion aggregation in high salt solutions. II. spectral graph analysis of water hydrogen-bonding network and ion aggregate structures, *J. Chem. Phys.* **141**, 154502 (2014).
- [37] J.-H. Choi and M. Cho, Ion aggregation in high salt solutions. VI. spectral graph analysis of chaotropic ion aggregates, *J. Chem. Phys.* **145**, 174501 (2016).
- [38] S. Sundar, A. A. Sandilya, and M. H. Priya, Unraveling the influence of osmolytes on water hydrogen-bond network: From local structure to graph theory analysis, *J. Chem. Inf. Model.* **61**, 3927 (2021).
- [39] F. M. Dietrich, X. R. Advincula, G. Gobbo, M. A. Bellucci, and M. Salvalaglio, Machine learning nucleation collective variables with graph neural networks, *J. Chem. Theory Comput.* **20**, 1600 (2024).
- [40] See Supplemental Material at <http://link.aps.org/supplemental/10.1103/PhysRevB.110.014105> for simulation settings and additional analysis.
- [41] L. Lutterotti and P. Scardi, Simultaneous structure and size-strain refinement by the Rietveld method, *J. Appl. Crystallogr.* **23**, 246 (1990).
- [42] R. Wang, M. DelloStritto, R. C. Remsing, V. Carnevale, M. L. Klein, and E. Borguet, Sodium halide adsorption and water structure at the α -alumina(0001)/water interface, *J. Phys. Chem. C* **123**, 15618 (2019).
- [43] C. Wang, H. Lu, Z. Wang, P. Xiu, B. Zhou, G. Zuo, R. Wan, J. Hu, and H. Fang, Stable liquid water droplet on a water monolayer formed at room temperature on ionic model substrates, *Phys. Rev. Lett.* **103**, 137801 (2009).
- [44] M. Parrinello and A. Rahman, Polymorphic transitions in single crystals: A new molecular dynamics method, *J. Appl. Phys.* **52**, 7182 (1981).
- [45] S. Nosé and M. L. Klein, Constant pressure molecular dynamics for molecular systems, *Mol. Phys.* **50**, 1055 (1983).
- [46] S. Nosé, A molecular dynamics method for simulations in the canonical ensemble, *Mol. Phys.* **52**, 255 (1984).
- [47] W. G. Hoover, Canonical dynamics: Equilibrium phase-space distributions, *Phys. Rev. A* **31**, 1695 (1985).
- [48] B. Hess, P-LINCS: A parallel linear constraint solver for molecular simulation, *J. Chem. Theory Comput.* **4**, 116 (2008).
- [49] U. Essmann, L. Perera, M. L. Berkowitz, T. Darden, H. Lee, and L. G. Pedersen, A smooth particle mesh Ewald method, *J. Chem. Phys.* **103**, 8577 (1995).
- [50] R. T. Cygan, J.-J. Liang, and A. G. Kalinichev, Molecular models of hydroxide, oxyhydroxide, and clay phases and the development of a general force field, *J. Phys. Chem. B* **108**, 1255 (2004).
- [51] H. Heinz, R. A. Vaia, B. L. Farmer, and R. R. Naik, Accurate simulation of surfaces and interfaces of face-centered cubic metals using 12-6 and 9-6 Lennard-Jones potentials, *J. Phys. Chem. C* **112**, 17281 (2008).
- [52] H. J. C. Berendsen, J. R. Grigera, and T. P. Straatsma, The missing term in effective pair potentials, *J. Phys. Chem.* **91**, 6269 (1987).
- [53] Y. K. Choi, N. R. Kern, S. Kim, K. Kanhaiya, Y. Afshar, S. H. Jeon, S. Jo, B. R. Brooks, J. Lee, E. B. Tadmor, H. Heinz, and W. Im, CHARMM-GUI nanomaterial modeler for modeling and simulation of nanomaterial systems, *J. Chem. Theory Comput.* **18**, 479 (2022).

- [54] M. J. Abraham, T. Murtola, R. Schulz, S. Páll, J. C. Smith, B. Hess, and E. Lindahl, GROMACS: High performance molecular simulations through multi-level parallelism from laptops to supercomputers, *SoftwareX* **1**, 19 (2015).
- [55] N. Michaud-Agrawal, E. J. Denning, T. B. Woolf, and O. Beckstein, MDAnalysis: A toolkit for the analysis of molecular dynamics simulations, *J. Comput. Chem.* **32**, 2319 (2011).
- [56] W. Humphrey, A. Dalke, and K. Schulten, VMD: Visual molecular dynamics, *J. Mol. Graphics* **14**, 33 (1996).
- [57] J. D. Hunter, Matplotlib: A 2D graphics environment, *Comput. Sci. Eng.* **9**, 90 (2007).
- [58] A. Luzar and D. Chandler, Structure and hydrogen bond dynamics of water-dimethyl sulfoxide mixtures by computer simulations, *J. Chem. Phys.* **98**, 8160 (1993).
- [59] A. P. Willard and D. Chandler, Instantaneous liquid interfaces, *J. Phys. Chem. B* **114**, 1954 (2010).
- [60] E. Duboué-Dijon and D. Laage, Characterization of the local structure in liquid water by various order parameters, *J. Phys. Chem. B* **119**, 8406 (2015).
- [61] D. Granata and V. Carnevale, Accurate estimation of the intrinsic dimension using graph distances: Unraveling the geometric complexity of datasets, *Sci. Rep.* **6**, 31377 (2016).
- [62] M. J. DelloStritto, S. M. Piontek, M. L. Klein, and E. Borguet, Effect of functional and electron correlation on the structure and spectroscopy of the $\text{Al}_2\text{O}_3(001)\text{-H}_2\text{O}$ interface, *J. Phys. Chem. Lett.* **10**, 2031 (2019).
- [63] R. Wang, Y. Zou, R. C. Remsing, N. O. Ross, M. L. Klein, V. Carnevale, and E. Borguet, Superhydrophilicity of α -alumina surfaces results from tight binding of interfacial waters to specific aluminols, *J. Colloid Interface Sci.* **628**, 943 (2022).
- [64] J. D. Cyran, M. A. Donovan, D. Vollmer, F. Siro Brigiano, S. Pezzotti, D. R. Galimberti, M.-P. Gageot, M. Bonn, and E. H. G. Backus, Molecular hydrophobicity at a macroscopically hydrophilic surface, *Proc. Natl. Acad. Sci. USA* **116**, 1520 (2019).
- [65] P. Grassberger and I. Procaccia, Measuring the strangeness of strange attractors, *Physica D* **9**, 189 (1983).
- [66] R. Ma, D. Cao, C. Zhu, Y. Tian, J. Peng, J. Guo, J. Chen, X.-Z. Li, J. S. Francisco, X. C. Zeng, L.-M. Xu, E.-G. Wang, and Y. Jiang, Atomic imaging of the edge structure and growth of a two-dimensional hexagonal ice, *Nature (London)* **577**, 60 (2020).
- [67] V. Kapil, C. Schran, A. Zen, J. Chen, C. J. Pickard, and A. Michaelides, The first-principles phase diagram of monolayer nanoconfined water, *Nature (London)* **609**, 512 (2022).
- [68] J. Jiang, Y. Gao, W. Zhu, Y. Liu, C. Zhu, J. S. Francisco, and X. C. Zeng, First-principles molecular dynamics simulations of the spontaneous freezing transition of 2D water in a nanoslit, *J. Am. Chem. Soc.* **143**, 8177 (2021).
- [69] W. Zhao, Y. Sun, W. Zhu, J. Jiang, X. Zhao, D. Lin, W. Xu, X. Duan, J. S. Francisco, and X. C. Zeng, Two-dimensional monolayer salt nanostructures can spontaneously aggregate rather than dissolve in dilute aqueous solutions, *Nat. Commun.* **12**, 5602 (2021).
- [70] T. Sato, T. Sasaki, J. Ohnuki, K. Umezawa, and M. Takano, Hydrophobic surface enhances electrostatic interaction in water, *Phys. Rev. Lett.* **121**, 206002 (2018).
- [71] S. Fayfar, A. Bretaña, and W. Montfrooij, Protected percolation: a new universality class pertaining to heavily-doped quantum critical systems, *J. Phys. Commun.* **5**, 015008 (2021).
- [72] A. Suma, D. Sigg, S. Gallagher, G. Gonnella, and V. Carnevale, Ion channels in critical membranes: Clustering, cooperativity, and memory effects, *PRX Life* **2**, 013007 (2024).
- [73] M. Farshad, M. J. DelloStritto, A. Suma, and V. Carnevale, Detecting liquid-liquid phase separations using molecular dynamics simulations and spectral clustering, *J. Phys. Chem. B* **127**, 3682 (2023).